International Journal of Solids and Structures 273 (2023) 112221

Contents lists available at ScienceDirect

International Journal of Solids and Structures

journal homepage: www.elsevier.com/locate/ijsolstr

Modeling fracture of multidirectional thin-ply laminates using an anisotropic phase field formulation at the macro-scale

Anatoli Mitrou [a], Albertino Arteiro [a], José Reinoso [b], Pedro P. Camanho [a,*]

[a] DEMec, Faculdade de Engenharia, Universidade do Porto, Rua Dr. Roberto Frias, s/n, 4200-465 Porto, Portugal
[b] Departamento de Mecánica de Medios Continuos y Teoría de Estructuras, School of Engineering, Universidad de Sevilla, Camino de los Descubrimientos s/n, 41092 Seville, Spain

ARTICLE INFO

Keywords:
Composite materials
Anisotropic
Failure
Laminate
Phase field

ABSTRACT

An equivalent single layer approach to model fracture events of multidirectional balanced thin-ply laminates via the use of the Phase Field method is explored. The inherent anisotropic nature of a multidirectional laminate is taken into account through the use of a structural tensor, defined from scaled directional vectors, which can account for the variation in fracture toughness of the laminates in varying directions. The scaling constants are defined using the lay-up of the laminate and the intra-laminar fracture toughness of the lamina, minimizing the number of input parameters required while also alleviating the structural tensor of a pure numerical and geometric meaning. They have a significant effect in the solution, and are here related to materials properties, not only providing a new perspective on their definition but also allowing the reduction of the number of numerical parameters used to calibrate the anisotropic PF model. The numerical implementation of the proposed formulation is performed using a simple and robust thermal analogy in Abaqus by exploiting the use of an anisotropic conductivity matrix that plays the role of the structural tensor in the anisotropic phase field formulation, which reduces the complexity of the simulations. Experimental results, based on open-hole tension and double edge-notched tension, are reproduced via simulation validating the model for size effects and for the response to off-axis loading. Successful prediction of notch size effects in multidirectional composite laminates is achieved by means of an equivalent single layer approach, incl. the off-axis open-hole tension strengths of a directional thin-ply laminate. All numerical strength predictions were well within acceptable errors of the respective experimental values.

1. Introduction

Carbon fiber reinforced polymer (CFRP) laminates have for years attracted the aerospace community due to their high strength to weight ratio that can lead to significant structural mass savings in conventional designs. Commonly, they consist of sequences of stacked unidirectional (UD) plies that have thicknesses around or above 0.125 mm. However, advancements in tow spreading techniques (Kawabe et al., 1998) brought into play much thinner plies, down to 15 μm (i.e., 0.0015 mm), resulting in what is called thin-ply composites. The fracture profile of such thin-ply composites differs significantly from that of standard CFRPs as was shown by various experimental studies during the emergence of thin-ply composites (Kawabe et al., 1998; Sihn et al., 2007; Tsai et al., 2005; Yokozeki et al., 2010). Fiber-dominated events are most prominent that macroscopically lead to a quasi-brittle response (Arteiro et al., 2020; Tsai et al., 2005), with the resulting crack pattern having the form of a single fracture plane upon which any damage mechanisms that occur can be assumed lumped on. This simplifies the analysis and thus motivated, for this particular type of CFRPs, the use of methods tied to the fracture of quasi-brittle materials, in an equivalent single layer (ESL) approach (Arteiro et al., 2019; Reinoso et al., 2017).

Laminate level analysis has generally been linked to analytical techniques to provide quick estimates for component sizing, such as the early work of Whitney and Nuismer (1974) based on the use of stress-based criteria for strength prediction, and, more recently, the work using finite fracture mechanics of Camanho et al. (2012). These approaches can provide accurate strength predictions in boundary value problems where the stress field and the stress intensity factor can be calculated analytically. More complex cases require a ply-by-ply discretization and different modeling approaches such as continuum

* Corresponding author.
E-mail address: pcamanho@fe.up.pt (P.P. Camanho).

https://doi.org/10.1016/j.ijsolstr.2023.112221
Received 16 September 2022; Received in revised form 17 March 2023; Accepted 18 March 2023
Available online 22 March 2023

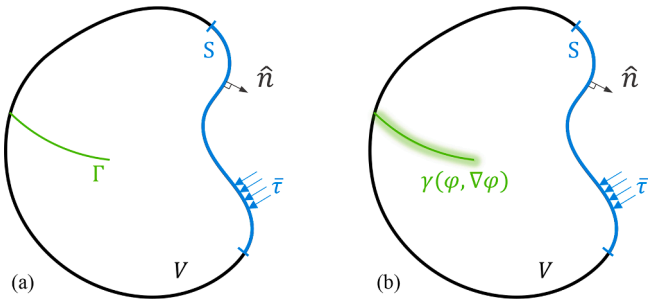

Fig. 1. Schematic solid (a) in a typical form (b) with the introduction of the PF (diffuse crack).

damage mechanics (Laux et al., 2021; Maimí et al., 2007; Schuecker and Pettermann, 2006; van der Meer et al., 2010) and the extended finite element method (XFEM) (Belytschko and Black, 1999; Iarve et al., 2011; Moes et al., 1999; Reifsnider et al., 2020). Other approaches, such as the cohesive zone modeling (CZM) (Turon et al., 2006), are mainly used to model to model delamination in multidirectional (MD) laminates. The application of XFEM and CZM methods using an ESL approach would rely on the use of the laminate fracture toughness, a property that is not straightforwardly identified in MD laminates subjected to general loading scenarios. The Phase Field (PF) approach to fracture, which was first applied at an ESL level to thin-ply laminates fracture by Reinoso et al. (2017), alleviates the need for predefined fracture planes, and it is well-suited to represent anisotropic behavior, both in the elastic properties and in the fracture toughness.

The PF method can be conceived as a global energetic approach to fracture stemming from the variational expression of Griffith's energy balance. This methodology was seminally introduced by Francfort and Marigo (1998), and Bourdin et al (2000). later formulated its regularized form to enable its numerical application. Since then, the PF method has been applied satisfactorily to a wide range of problems, see (Ambati et al., 2015; Carollo et al., 2018; Nguyen et al., 2017; Raina and Miehe, 2016) and the references therein. However, with regards to a macroscopic representation of MD composite laminates, remarkable challenges stemming from the accurate representation of their anisotropic nature remain, both concerning the elastic response and the fracture energy during the failure process. This is something the pioneering work of Reinoso et al. (2017) did not have to actively pursuit as it only addressed quasi-isotropic (QI) laminates, which significantly simplified the problem from this perspective.

Among the first to formulate an anisotropic PF model were Clayton and Knap (2015), applying it to fracture of polycrystals that presented preferred fracture planes. The authors introduced the addition of a structural tensor to restrict damage to these preferred planes by penalizing damage on all other planes. Their method was later used in multiple works, including that of Nguyen et al. (2017) that used the same idea adding multiple phase field variables restricted to respective planes in polycrystals, and Teichtmeister et al. (2017) that fully explored and mathematically explained this approach to modeling fracture energy anisotropy. Bleyer and Alessi (2018), Quintanas-Corominas et al. (2019) and Pillai et al. (2020) also used individual phase field variables, each restricted to a specific direction, in order to model independent damage mechanisms that occur in UD composites (or at the ply level), i.e., transverse and longitudinal damage, while also addressing anisotropic degradation of the stiffness matrix. In all the aforementioned applications, whether referring to a fracture plane or a damage mechanism, what is known *a posteriori* is the exact plane each phase field variable will act on. However, these anisotropic PF approaches present significant shortcomings for a direct use in the case of a MD thin-ply laminate, modeled at the macroscopic level, i.e., with an ESL representation, as they cannot be used in a similar manner, since such a split between the different damage mechanisms cannot be assumed, and all of them are lumped into an equivalent crack at the laminate level, whose plane is an active unknown in the analysis.

Taking notice of that, this work aims at providing a different perspective in applying the PF method to general, not necessarily QI, MD laminates. This entails inherently linking the anisotropic nature of MD laminates to the anisotropic PF model without defining fracture paths *a priori*. Instead, the crack path should result from the fracture toughness of the laminate along its principal orthotropy directions and from the anisotropic PF model (Teichtmeister et al., 2017). The theoretical aspects and proposed formulation are explained in Section 2 that is followed by the presentation of distinctive numerical results, which are compared to experimental data from the literature, to demonstrate the capability of the model in Section 3. It is noted that the mathematical convention used has matrices represented by a bold capital letter in non-italic (i.e., **C**), vectors bold and italic (i.e.,$\boldsymbol{n}$) and scalars simple italic (i.e., x).

2. Theoretical aspects

2.1. Anisotropic phase field fracture model

The PF approach to fracture is based on the minimization of the total potential energy of a cracked solid. Consider the solid of volume, V, that contains a crack, Γ, with external tractions, $\bar{\boldsymbol{\tau}}$, applied to part of its boundary, S, defined by the normal vector $\hat{\boldsymbol{n}}$, as seen in Fig. 1. Assuming no body forces act on the volume the total potential energy, complying with Griffith's representation of fracture, has the form:

$$\Pi(\boldsymbol{u}) = U_e + U_f - W \tag{1}$$

where W is the work of external forces and tractions, U_e is the bulk elastic energy and U_f is the surface energy related to the crack, defined as:

$$U_f = \int_{\Gamma} G_c d\Gamma \tag{2}$$

where G_c is the fracture toughness. The unknown nature of the crack geometry, Γ, does not allow the numerical solution of the problem, so, to circumvent that, a scalar-based phase field variable, $\varphi = \varphi(x)$, is introduced. This variable is a scalar that takes the value of zero in a pristine state and the value of one in a fully damaged state, allowing the crack to be represented in a diffuse manner (Fig. 1(b)). This means that the surface energy can be represented by a volumetric integral of a surface energy density function, $\gamma(\varphi, \nabla\varphi, \mathbf{A})$, which now represents the crack (Eq. (3):

$$U_f = \int_{\Gamma} G_c d\Gamma \approx \int_{V} g_c \gamma(\varphi, \nabla\varphi, A) dV \tag{3}$$

where g_c is a parameter that does not intrinsically hold a physical meaning, but in the case that the material is isotropic it takes the value of the Mode I fracture toughness of the material, G_c, and **A** is a 2nd order structural tensor, which enables the representation of an anisotropic fracture energy (Teichtmeister et al., 2017). This formulation is often referred to as a 1st order anisotropic PF model. The isotropic case is recovered if **A** is equal to the identity tensor, **I**. More details on **A** and how it is formulated will be elaborated in Section 2.3.

The form of the crack surface density function, γ, is given by Ambrossio-Tortorelli (AT) functionals, in a regularized form, in the general sense of Γ-convergence (i.e., a certain functional will tend to another when the regularizing parameter tends to zero, so how well Eq. (3) holds) as presented and formulated by Bourdin et al. (2000), and taking into account anisotropy (Teichtmeister et al., 2017), as:

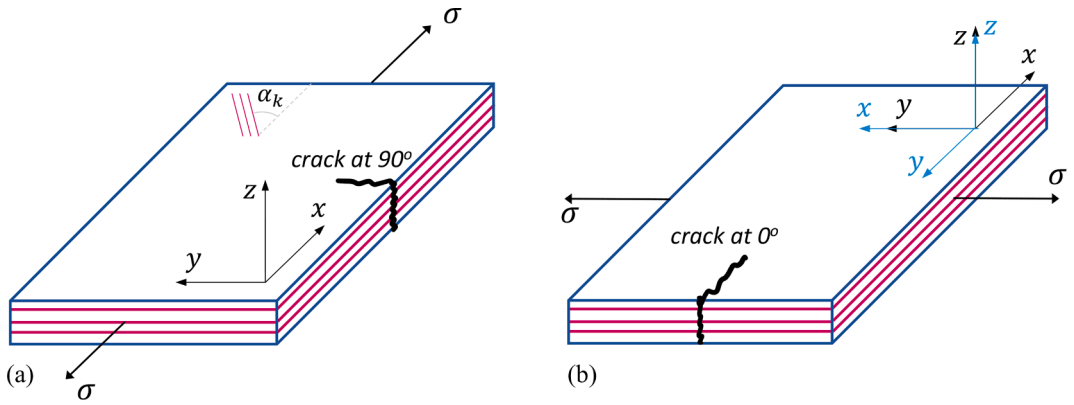

Fig. 2. Schematic of the plate (a) loaded along the 0° plies, and (b) loaded perpendicularly to the original 0° plies giving the fracture toughness for a crack moving at 0° with respect to the initial reference frame.

$$\gamma(\varphi, \nabla\varphi, \mathbf{A}) = \frac{1}{4c_w l}\left(\omega(\varphi) + l^2 \nabla\varphi \cdot \mathbf{A} \cdot \nabla\varphi\right) \tag{4}$$

where c_w is a constant given by $\int_0^1 \sqrt{\omega(\varphi)}d\varphi$, and $\omega(\varphi)$ is a function that by default is given based on the AT functional used to define $\gamma(\varphi, \nabla\varphi, \mathbf{A})$, and must satisfy the conditions: $\omega(0) = 0$ and $\omega(1) = 1$, with the two most commonly seen forms $\omega(\varphi) = \varphi$ (i.e., AT1 model) and $\omega(\varphi) = \varphi^2$ (i.e., AT2 model), as seen in the literature. l is the regularization parameter, or length scale as it is often referred to.

The length scale can either be interpreted as a purely numerical parameter or as an internal characteristic length. The latter was initially argued by Pham et al. (2011), who linked the PF method to gradient damage models, expressing the length scale in terms of the strength, fracture toughness, and elastic modulus of the material. Recently, Molnár et al. (2020) considered defining it in terms of characteristic lengths that occur in other theoretical fracture models such as finite fracture mechanics. Inevitably the results obtained by a PF simulation, using such approximations, are dependent on the value of the length scale (Tanné et al., 2018). This, especially with regards to experimental correlation, is the *Achille's heel* of the method as a clear consensus does not yet exist on what is more appropriate, and so, care must always be given to the selection and use of the length scale parameters. The models proposed by Wu (2017) and Lorentz (2017), which recover a cohesive zone model, detach the method from a length scale dependency, by rendering the strength the explicit material input, however, a restriction remains with regards to its relation to the overall geometrical dimensions (Lorentz, 2017). Proper understanding of the intricacies of each approach is, thus, imperative for appropriate use and selection.

The elastic energy, U_e, also changes with the introduction of the PF variable and becomes:

$$U_e = \int_V g(\varphi)\frac{1}{2}\boldsymbol{\varepsilon}^T \cdot \mathbf{C} \cdot \boldsymbol{\varepsilon} dV \tag{5}$$

where $\mathbf{C}$ is the material stiffness matrix, $\boldsymbol{\varepsilon}$ is the infinitesimal strain tensor (in a vector form) and $g(\varphi)$, is the degradation function, a function that degrades the stiffness of the material as damage occurs. In this work, the quadratic form $g(\varphi) = (1-\varphi)^2$ is used.

Lastly, the governing equations of the problem in the strong form are obtained by applying the principle of virtual work to Eq. (1). Considering $U = U_e + U_f$, and $\boldsymbol{\sigma}$ the stress tensor (in a vector form), given as $\boldsymbol{\sigma} = \mathbf{C} \cdot \boldsymbol{\varepsilon}$, the following Euler-Lagrange equations (Eq. (6a)) and natural boundary conditions (Eq. (6b)) are obtained:

$$\begin{aligned} &\nabla \bullet \boldsymbol{\sigma} = 0 && \text{in } V \\ &\nabla \bullet \left(\frac{\partial U}{\partial \nabla\varphi}\right) - \frac{\partial U}{\partial \varphi} = 0 && \text{on } S \end{aligned} \tag{6a}$$

and

$$\begin{aligned} &\boldsymbol{\sigma} \cdot \hat{\boldsymbol{n}} = \bar{\boldsymbol{\tau}} && \text{in } V \\ &\left(\frac{\partial U}{\partial \nabla\varphi}\right) \cdot \hat{\boldsymbol{n}} = 0 && \text{on } S \end{aligned} \tag{6b}$$

All but the second Euler-Lagrange equation, which is the one that governs the damage evolution and is, thus, often referred to as the evolution equation, are not fully developed here to remain concise. Substituting Eq.2 through Eq.5 into Eq.6a (second terms), one gets:

$$\frac{g_c}{4c_w l}\left(\frac{\partial \omega(\varphi)}{\partial \varphi} - 2l^2 \nabla \cdot (\mathbf{A} \cdot \nabla\varphi)\right) + \frac{\partial g(\varphi)}{\partial \varphi} W_e = 0 \tag{7}$$

where W_e is the undamaged elastic energy defined as $\frac{1}{2}\boldsymbol{\varepsilon}^{\mathrm{T}} \cdot \mathbf{C} \cdot \boldsymbol{\varepsilon}$. Assuming the damage model AT2 and the quadradic degradation function, as used for the analysis in this work, the previous equation becomes:

$$\frac{g_c}{l}\left(\varphi - l^2 \nabla \cdot (\mathbf{A} \cdot \nabla\varphi)\right) - 2(1-\varphi)W_e = 0 \tag{8}$$

The evolution equation was developed here to the form of Eq. (8) as it is important for the application of the method within a Finite Element Analysis (FEA) context, as will be explained in Section 3. It should be noted that for Eq. (8) to fully define the damage evolution, an irreversibility of damage, i.e., $\dot{\varphi} \geq 0$, must be ensured. In order to comply with this condition, within the numerical implementation, we use the history variable proposed by Miehe et al. (2010) defined as:

$$H = \max\left(W_e^{t_0}, W_e^t\right) \tag{9}$$

where t_0 is the total time at the start of the current increment, and t is the current time of the incrementation step. The history variable, that takes the place of W_e in Eq. (8), satisfies the Karush-Kuhn-Tucker conditions:

$$W_e^t - H \leq 0, \dot{H} \geq 0, \dot{H}\left(W_e^t - H\right) = 0 \tag{10}$$

2.2. Fracture toughness of multidirectional balanced laminates

Defining the inputs for the PF method from a mechanical standpoint becomes straightforward when considering the elastic properties of the material using classical approaches such as the classical laminated plate theory (CLPT) (Braun et al., 1994; Christensen and Zywicz, 1990; Sun and Li, 1988). However, addressing fracture toughness is not as direct. For MD laminates, the fracture toughness will vary depending on the crack plane orientation, so a way to account for this effect needs to be defined. The work of Camanho and Catalanotti (2011) is used here to capture the relation between each orientation and fracture toughness. In this work, the authors defined the Mode I intra-laminar fracture toughness of a MD laminate, i.e., assuming a crack moving perpendicularly to the load application direction, using analytical terms that

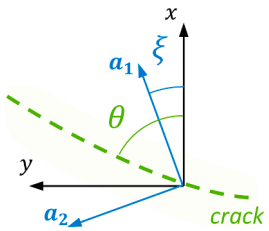

Fig. 3. Schematic of the assumed angles in the proposed formulation.

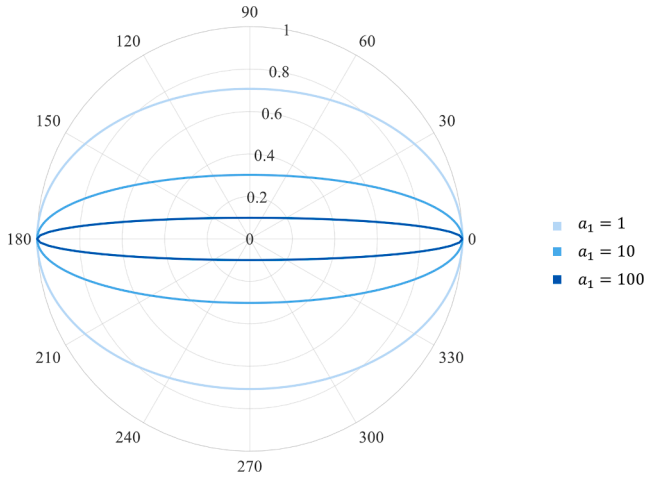

Fig. 4. Polar plot of the reverse of $G_c(\theta)$ assuming a unit value for g_c and $a_1 = 1, 10, 100$ and $a_2 = 0$.

require the intra-laminar fracture toughness only, G_c^0, and elastic constants of a 0° ply (lamina), and the lay-up of the laminate.

Consider the plate shown in Fig. 2(a) and the corresponding global reference frame (x, y, z), which corresponds to the principal axes of orthotropy of the laminate. The 0° plies lie in the loading direction which is coincident with the direction of the x-axis, while the rest of the plies are at an angle α_k with the x-axis, where k is the index used to denote each occurring balanced sublaminate. The fracture toughness of the laminate, G_c^L, for a crack moving along the y-axis, is then given by (Camanho and Catalanotti, 2011):

$$G_c^L = \sum_{k=1}^{n} G_c^k v_k = G_c^0 E_{eq}^0 \sum_{k=1}^{n} \left(\Omega_k \frac{\chi_k}{\chi_0}\right)^2 \frac{v_k}{E_{eq}^k} \tag{11}$$

where:

$$E_{eq} = \frac{\sqrt{E_x E_y}}{\sqrt{\sqrt{\frac{E_y}{E_x}} + \frac{E_y}{2G_{xy}} - \nu_{xy}}} \tag{12}$$

where E_x and E_y are the elastic moduli in the principal orthotropy frame, G_{xy} is the shear modulus, ν_{xy} and ν_{yx} are the corresponding Poisson's ratios, $k = 1 \cdots n$, where n is the total number of balanced sublaminates, G_c^k is the Mode I fracture toughness of the balanced sublaminate, k, for a crack propagating along the y-direction, v_k is the ratio of the sublaminate thickness and the total thickness of the laminate, Ω_k is the stress ratio between the 0° ply and balanced sublaminate, k, calculated from CLPT, and χ_k and χ_0 are the orthotropy correction factors for the sublaminate and 0° ply, respectively, given by (Bao et al., 1992):

$$\chi = \frac{1 + 0.1(\rho - 1) - 0.016(\rho - 1)^2 + 0.002(\rho - 1)^3}{\left(\frac{1+\rho}{2}\right)^{1/4}} \tag{13}$$

where:

$$\rho = \frac{\sqrt{E_x E_y}}{2G_{xy}} - \sqrt{\nu_{xy}\nu_{yx}} \tag{14}$$

2.3. Anisotropic scaling constants

It is expected that a generally layered MD laminate will have an orientation dependent fracture toughness $G_c(\theta)$. To account for the variation in the fracture toughness for a MD laminate within the PF model the derivation presented in the previous subsection is now linked to the second-order structural tensor $\mathbf{A}$ that governs the damage form and effective fracture toughness of the solid. As explained in the work of Teichtmeister et al. (2017), the structural tensor can be used to account for particular levels of fracture energy anisotropy that are linked to intrinsic material symmetries. The intrinsic material symmetries are represented by an orthogonal system of what is referred to as preferred directions (or planes). For the case of an orthotropic material, such as a balanced laminate, the structural tensor can be defined considering two directions, $\boldsymbol{a}_1$, $\boldsymbol{a}_2$, as:

$$\mathbf{A} = \mathbf{1} + a_1 \boldsymbol{a}_1 \otimes \boldsymbol{a}_1 + a_2 \boldsymbol{a}_2 \otimes \boldsymbol{a}_2 \tag{15}$$

where a_1 and a_2 are two scaling constants corresponding to the respective scaled preferred directions. Teichtmeister et al. (2017) showed that these constants significantly influence the crack path and effective fracture toughness (expressed in terms of the critical energy release rate (ERR)). As explained in the work of Li et al. (2015), the variational nature of the PF method inherently assumes that crack propagation is governed by a maximum energy release rate (MERR) criterion that will provide the angle at which the fracture plane will be oriented. Intuitively, this can be demonstrated by finding the point at which the polar plot of the inverse of the fracture toughness, $G_c(\theta)$, intersects a line that follows the load direction. For more details on this, the reader is referred to Li et al. (2015) and Teichtmeister et al. (2017) and the references therein. Considering ξ the angle of $\boldsymbol{a}_1$ respective to the global x-axis, and θ the angle that the crack follows respective to the global x-axis (Fig. 3), the fracture toughness as a function of these angles is given through an energetic balance as (Teichtmeister et al., 2017):

$$G_c(\theta, \xi) = g_c \sqrt{\frac{l^*}{l}} \tag{16}$$

where l^* is the effective length scale that is given by:

$$l^* = l\left(1 + a_1 \sin^2(\theta - \xi) + a_2 \cos^2(\theta - \xi)\right) \tag{17}$$

It is noted that the length scale, and corresponding effective length scales, must be sufficiently small compared to the dimensions of the domain (i.e., the overall dimensions of the modelled component) for this representation of anisotropic fracture energy to have meaningful effect in the analysis (Scherer et al., 2022; Teichtmeister et al., 2017). In cases where the domain is significantly larger than the length scale, the solution localizes and, due to this, directionality becomes pertinent. Therefore, the use of the structural tensor to provide anisotropic considerations for the fracture energy refers to only such cases, a fact that was also addressed in Teichtmeister et al. (2017). When the length scale approaches in size the dimensions of the domain, a homogeneous solution is achieved, and a fully failed domain is obtained. In that sense, having anisotropic fracture energy would not pose any reasonable effect since directionality dependence is in effect lost. This was in fact shown by the recent work in Scherer et al. (2022). To preserve an effect of anisotropy, Scherer et al. (2022) used a model based on the work of Bleyer and Alessi (2018) and had anisotropic stiffness degradation linked to the evolution of the phase field variable. However, as pointed out before, the work of Bleyer and Alessi (2018), is based on known paths of damage formation and, thus, imposition of a corresponding degradation in the stiffness based on the independent evolution of the respective PF variables, is possible. But, in a problem, such as the one

studied here where predefined failure planes do not exist, directionally dependent stiffness degradation cannot be considered. Since the application in this work refers to a macro-scale, component level analysis, this is not considered a limitation or concern since Scherer et al. (2022) that compared both approaches for the localized solution, showed that for a localized solution and the level of anisotropy considered here similar results are obtained.

If the principal axes of orthotropy are considered to coincide with the global reference frame (i.e., global x,y axis system), as is done in this work, $\xi = 0$ in Eq. (17) giving a direct distribution of the effective fracture toughness, $G_c = f(\theta)$:

$$G_c(\theta) = g_c\sqrt{1 + a_1\sin^2(\theta) + a_2\cos^2(\theta)} \tag{18}$$

As stated in the relevant references cited throughout this work, this refers to a case of weak anisotropy. It also becomes apparent that the scaling constants have direct influence on the fracture toughness distribution accounted for by the model. As demonstrated by Teichtmeister et al. (2017) for the specific case of a transversely isotropic material where $a_2 = 0$, the scaling constant a_1 plays the part of defining how strongly the crack follows the preferred direction. For instance, in Fig. 4, the polar plots of the reverse of the fracture toughness, $G_c(\theta)^{-1}$, for different values of a_1, keeping $a_2 = 0$ and are shown. As a_1 is given a larger value the "flatter" the ellipse of the inverse of the fracture toughness becomes, essentially maximizing the fracture toughness in the direction perpendicular to $\boldsymbol{a}_1$ (i.e., 90° in the plot).

However, as can be seen, a direct consequence of assuming transverse isotropy is that the toughness corresponding to the preferred direction $\boldsymbol{a}_1$ is independent of the value chosen for a_1. Thus, given a known plane of fracture and its fracture toughness, it is enough to set a sufficiently large value of a_1 to restrict damage in any direction that lies out of the preferred one, $\boldsymbol{a}_1$, by rendering the toughness too high in other directions to ever allow any damage. This was in fact the principle used by Clayton and Knap (2015), and later by other works (Bleyer and Alessi, 2018; Pillai et al., 2020; Quintanas-Corominas et al., 2019), to define the fracture energy anisotropy, in which the scaling constant held a purely numerical character since restriction of damage to specific directions was of interest.

In the orthotropic case though, where the path the crack will assume is not known *a priori* but is dependent on the values of the fracture toughness in the principal directions, $\boldsymbol{a}_1$, $\boldsymbol{a}_2$, and loading direction, the scaling constants must not be defined in the same numerical approach as in transverse isotropy. In that sense, the previous analytical framework for calculating the fracture toughness of MD balanced laminates can be directly used to calculate the scaling constants. This will render them material dependent and alleviate them of a purely numerical character, while also reducing the number of numerical parameters the model depends on. Using Eq. (18) for $G_c(\theta = 0^\circ)$ and $G_c(\theta = 90^\circ)$ the scaling constants a_1 and a_2 can be calculated based on the fracture toughness given by Eq. (11) for cracks moving in those directions. For clarity at this point, it is noted that when referring to $G_c^{L,0^\circ} = G_c(90^\circ)$ the calculation for the fracture toughness was done based on a load acting in the x-axis (i.e., 0°). To get $G_c^{L,90^\circ} = G_c(0^\circ)$ for the laminate the calculations in Eq. (11) are repeated but for the "rotated" coordinate system (i.e., the lay-up sequence is offset by 90°, Fig. 2(b)) with the load now acting along the y-axis. Thus, the scaling constants are given as:

$$a_1 = \left(\frac{G_c(90^\circ)}{g_c}\right)^2 - 1 = \left(\frac{G_c^{L,0^\circ}}{g_c}\right)^2 - 1 \tag{19a}$$

$$a_2 = \left(\frac{G_c(0^\circ)}{g_c}\right)^2 - 1 = \left(\frac{G_c^{L,90^\circ}}{g_c}\right)^2 - 1 \tag{19b}$$

Setting g_c equal to the fracture toughness of the 0° ply, $g_c = G_c^0$, and simplifying Eq. (19a) and (19b) the scaling constants become:

$$a_{1,2} = \left(E_{eq}^0 \sum_{0^\circ,90^\circ}\left(\Omega_k\frac{\chi_k}{\chi_0}\right)^2\frac{v_k}{E_{eq}^k}\right)^2 - 1 \tag{20}$$

where the subscript in the summation, denotes the orientation of load when the calculation of the fracture toughness is made as explained above, e.g., 0° refers to a load acting in the x-axis and the fracture toughness is for a crack moving along the y-axis. It is pointed out once again that the x-axis is considered to follow the 0° plies present in the laminate meaning the lay-up sequence is expressed in terms of angles with respect to the assumed x-axis. For the fracture toughness for a crack along the 0° direction the lay-up is essentially expressed with respect to the y-axis (Fig. 2(b)).

It becomes apparent that $a_{1,2}$ can be calculated solely based on the lay-up and elastic properties of the lamina and the fracture toughness of the 0° ply, which now become the inputs of the model. It is important to note that this derivation is valid for balanced laminates, assuming that the laminate fracture toughness can be obtained from the pure mode I fracture toughness along the two principal axes of orthotropy, following the specific simple form of the fracture toughness distribution obtained through the use of the second-order structural tensor from Teichtmeister et al. (2017). In other words, considerations of mixed-mode states to the total fracture toughness of the laminate are neglected in the current approach. Mixed-mode loading would require more intricate forms of the fracture toughness distribution and further exploration of the connection of fracture modes and elastic anisotropy. This will be highlighted in some of the examples that follow.

3. Representative applications and validation

3.1. Numerical implementation

The proposed PF model is implemented in the implicit solver Abaqus/Standard using a user defined material subroutine (UMAT), extending the implementation of Navidtehrani et al. (2021), with the addition of a user defined thermal behavior subroutine (UMATHT) to add the anisotropic considerations. The approach is based on an analogy of the PF problem to that of heat transfer for a solid with a temperature field T, for which a heat transfer process is governed by the following equation (Abaqus, 2020, 2019):

$$\int_V \left(\rho\dot{U} - \nabla\cdot(\mathbf{K}\cdot\nabla T)\right)dV = \int_{V_S} qdV_S + \int_V rdV \tag{21}$$

where V_S is the surface area of the solid, ρ is the density of the material, $\dot{U}$ is the material time rate of the internal energy, q is the heat flux per unit area of the body flowing into the body,r is the heat supplied internally into the body per unit volume, and, finally,$\mathbf{K}$ is the conductivity matrix (if isotropic conductivity is assumed then $\mathbf{K} = k\cdot\mathbf{I}$ and can thus be replaced by a scalar with the value of the uniform conductivity k). If steady state conditions and only volumetrically generated heat are assumed, $\dot{U} = 0$ and $q = 0$, and then Eq. (21) results in:

$$\int_V -\nabla\cdot(\mathbf{K}\cdot\nabla T)dV = \int_V rdV \tag{22}$$

which would lead to the governing Euler equation in the volume:

$$-\nabla\cdot(\mathbf{K}\cdot\nabla T) = r \tag{23}$$

However, from Eq. (8) we can get:

$$\nabla\cdot(\mathbf{A}\cdot\nabla\varphi) = \frac{\varphi}{l^2} - \frac{2(1-\varphi)}{g_c l}W_e \tag{24}$$

So, it becomes apparent that the Fourier law term $(\nabla\cdot(\mathbf{K}\cdot\nabla T))$ of Eq. (23) can be directly compared to the term $(\nabla\cdot(\mathbf{A}\cdot\nabla\varphi))$ of Eq. (24) (and Eq.7–8), thus the conductivity matrix can play the role of the structural

Table 1
Definition of required internal UMATHT variables.

Variable	Definition
u=	$u-(r/\rho)$
dudt=	0
dudg=	0
flux=	$-\mathbf{K}\cdot\nabla T$
dfdg=	$-\mathbf{K}$
dfdt=	0

tensor in the anisotropic PF formulation. To internally update the conductivity matrix (i.e., structural tensor) the UMATHT is added to treat the thermal behavior of the material. The history variable defined in Eq. (9) ensures the irreversibility condition of the PF variable. Specific to Abaqus, it is noted that the use of a UMATHT, that provides the definition of a user defined thermal behavior, requires specific mandatory variables to be defined. First and foremost, density must be defined in the input file, which is set equal to one to hold the thermal analogy. Within the UMATHT itself, the following variables must be defined: *u*, internal energy per unit mass; *dudt*, variation of thermal energy with respect to temperature; *dudg*, variation of thermal energy with respect to gradients of temperature; *flux*; heat flux vector; *dfdt*, variation of the heat flux vector with temperature; and *dfdg*, variation of the heat flux vector with respect to temperature gradients, and equal to the conductivity. Their values and form, given to respect the heat transfer analogy for the PF implementation in Abaqus, is shown in Table 1.

After defining the UMATHT following the guidelines above, it can be used in a straightforward manner as an addition to the UMAT formulated by Navidtehrani et al. (2021) from which all other aspects, presented for the isotropic case, still hold, making this a rather robust and simple implementation of the anisotropic PF method for FEA. To the best of the authors' knowledge, this extension has not been done so far. The ability to alter the structural tensor internally, as it is another variable requiring definition, not only allows the application of this methodology but also adds additional versatility in potential applications, e.g., application of a maximum principal stress or strain fracture criterion to define fracture planes, all while keeping the benefit of using Abaqus's built-in elements and features.

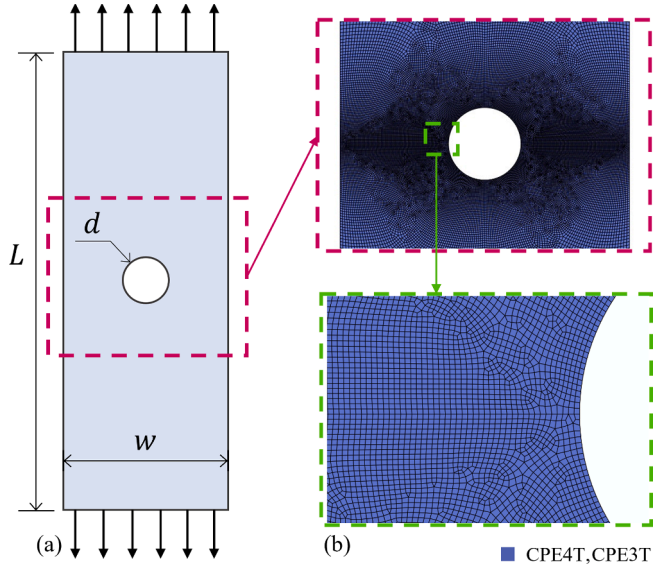

Fig. 5. (a) OHT specimen configuration and (b) discretization followed around the hole.

Table 2
Material properties for the T700/AR-2527 lamina and laminate of Lay-up 1.

	E_x(GPa)	E_y(GPa)	G_{xy}(GPa)	ν_{xy}
Lamina	111.0	7.4	4.2	0.3
Laminate	42.402	42.402	16.241	0.3

3.2. Verification with experimental results

3.2.1. Size effects

3.2.1.1. Open hole tension. An initial step towards the validation of the proposed formulation is based on the experimental results presented by (Arteiro et al., 2013). The authors tested laminates manufactured with thin-plies in an Open-Hole Tension (OHT) configuration that is shown in Fig. 5. The model is implemented in Abaqus and plane strain elements CPE4T and CPE3T are used for the discretization. As mentioned in Section 3.1 the temperature degree of freedom is necessary to implement the PF method (i.e., due to the analogy between the governing equations of the temperature and PF variable). The full details about the experiments can be found in Arteiro et al. (2013) and are omitted here for the sake of brevity. The results for Lay-up 1, $[(0/-45)/(0/45)]_{6T}$, a QI laminate of NCF C-Ply™ T700/AR-2527 epoxy system, with the lamina and equivalent laminate properties reported in Table 2 (x denotes the longitudinal and y the transverse direction respectively) are considered. The equivalent properties are computed using a weighted average approach of the mechanical properties over the thickness direction as explained in Braun et al. (1994), which is used to compute an equivalent stiffness, $\mathbf{C}$, for the laminate, in the general sense of macromechanical homogenization (Tsai, 2021). The intralaminar fracture toughness of the lamina, G_c^0, is 114.2 N/mm. The dimensions of the specimens are reported in Table 3.

Using these properties and following the process of Section 2.2-2.3 it is possible to obtain the orthotropic PF scaling constants for the structural tensor, $a_1 = a_2 = -0.9079$ (Eq. (20). As expected, the scaling constants are equal since the laminate is QI and the fracture toughness, 36.3 N/mm, is equal for all orientations, very close to the reported experimental value (Arteiro et al., 2013). The length scale in this work is taken as a numerical parameter that is obtained for a laminate by fitting a certain set of experimental results. For the QI laminate of these OHT experiments its value is chosen to be $l = 0.88$ mm and was calculated to fit the first set of experimental results (Size A) satisfactorily. The dependence of the obtained response on the value of the length scale is shown in Fig. 6(a) where the responses for $l = 0.40, 0.60, 0.88$ mm are all shown to illustrate the procedure. For the subsequent sizes the length scale is not altered to aid in assessing the ability of the model to predict size effects. As shown in Fig. 5(b), around the notch and along the line extending from the horizontal diameter, the finest mesh size is used (0.04 mm average element length). This was also kept as the minimum element size in the rest of the examples that follow.

Table 4 provides a comparison of the average measured strength and the strength predicted from FEA alongside the respective errors. Fig. 6 shows the comparison of the experimental and numerical stress versus displacement curves. As can be observed, the experimental results are captured well, with the strength prediction of Size B being the one that resulted in the highest error. These results highlight the ability of the model to capture size effects.

The crack form predicted from the simulation can be seen in Fig. 6

Table 3
Tested OHT specimen sizes.

	w(mm)	*d*(mm)	*L*(mm)
Size A	12	3	250
Size B	24	6	250
Size C	40	10	250

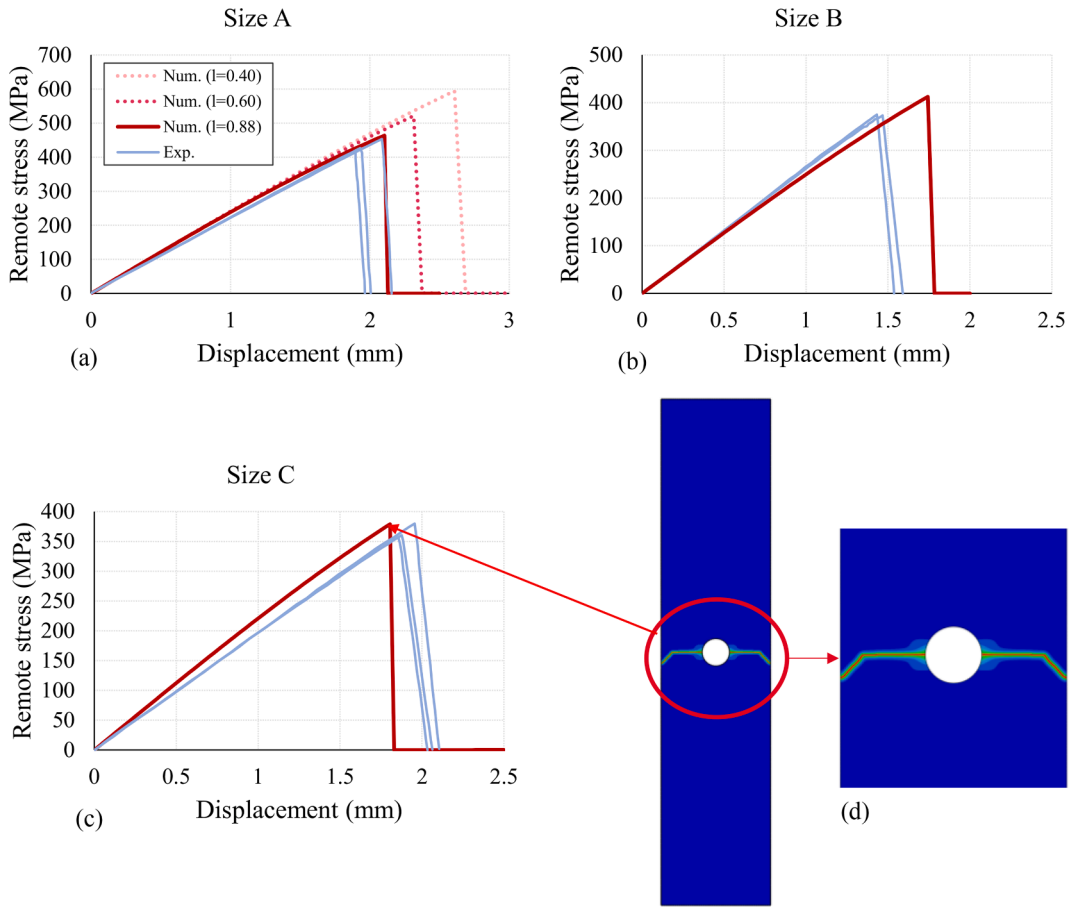

Fig. 6. OHT results (a) $w = 12$ mm (b) $w = 24$ mm (c) $w = 40$ mm (d) numerical fracture profile.

Table 4
OHT experimental and numerical results comparison.

	Experimental Av. (MPa)	FEA Prediction (MPa)	Error (%)
Size A	431.80	463.28	6.70
Size B	373.90	412.46	9.30
Size C	365.60	379.07	3.50

(d), shown specifically for the specimen of Size C. As seen in the experimental results shown in Fig. 7, the crack follows a straight path that lies along the axis perpendicular to the load application direction. In the simulation the same is observed. A deviation near the edge can be seen (Fig. 6(d)), which, after a study of the effect of different parameters of the simulation (e.g., model size, mesh, incrementation parameters), is attributed to inherent numerical instabilities of the solver. Fig. 8 shows OHT simulation results, for the same material and anisotropic model parameters, for a specimen with altered length, shorter compared with the original one (Fig. 6(d)). The effect near the edge decreases significantly. Despite this difference, the obtained strength remains the same. Thus, this observed deviation was not given any significance other than that of a numerical artifact that was attributed to the numerical solution scheme adopted to solve the coupled system of equations.

3.2.1.2. Double edge notched tension. In addition to the OHT results presented in Section 3.2.1.1, Double Edge-Notched Tension (DENT) experimental results are also reproduced. The experimental results are those from Furtado et al. (2020) that tested DENT cross-ply, $[0/90]_{ns}$, laminates of variable ply thicknesses of the T700/M21 material system. The experimental results for the system referred to as H75, with a ply thickness of 0.075 mm, of a lay-up of $[0/90]_{8s}$, are modeled. The material properties and specimen dimensions are seen in Table 5 and 6 respectively, while the configuration is shown in Fig. 9(a). Once again, the laminate elastic properties are calculated using the using a weighted average approach of the mechanical properties over the thickness direction by Braun et al. (1994). The value for the intra-laminar fracture toughness of the lamina is $G_c^0 = 67.0$ N/mm, reported as the initiation value in Furtado et al. (2020).

A similar modeling strategy as before is followed to set up the FE model, with a length scale of 1.2 mm being used, the one providing a satisfactory fit to the first set of experimental results for Size A. In this case, the scaling constants are given as $a_1 = a_2 = -0.075$. They turn out to be equal since the fracture toughness values used to obtain them refer to the principal axes of orthotropy of the material for which the laminate presents the same fracture toughness. Fig. 10 presents a comparison of the fracture toughness distribution for the laminate as obtained with the proposed PF formulation versus the virtual crack closure technique (VCCT) (Krueger, 2004). Please refer to Appendix A regarding the determination of the laminate fracture toughness distribution using VCCT.

It becomes apparent that the method properly captures the fracture toughness at directions coincident with the principal axes of orthotropy but does not succeed in other directions. This would require the use of more complex formulations, like the higher order methods as referred to by Li et al. (2015), Li and Maurini (2019), Scherer et al. (2022) and Teichtmeister et al. (2017). This significantly complicates the analysis and was not explored here because the objective is to capture the size effect on experimental results executed under on-axis loading for this laminate. Future experimentation and modeling efforts could improve this or shed light to what the best approach could be.

The strengths were predicted within acceptable errors and the

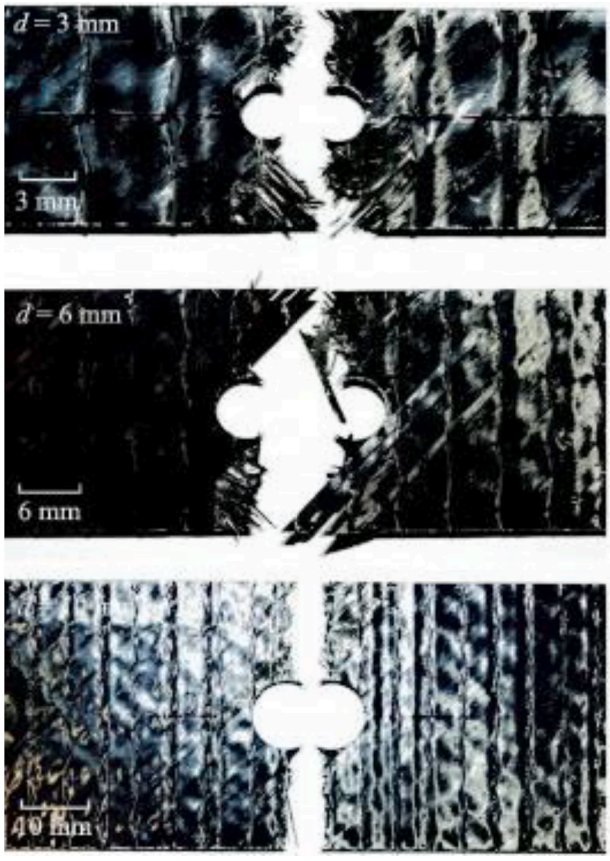

Fig. 7. Failed OHT specimens (Arteiro et al., 2013).

respective results can be seen in Table 7. The typical crack pattern, numerical and experimental, is shown in Fig. 9(b)-(c), respectively. It is noted that comparing the computational time required by the continuum damage model used by Furtado et al. (2020) and the PF model presented here, the latter achieves the same results within 25 % of the time the former requires, all awhile having a much simpler model set-up.

3.2.2. *Off-axis behavior*

The previous brief discussion on the accuracy of the representation of the variation of fracture toughness for a cross-ply laminate (Fig. 10) presents a limitation of the capability of the model if cases of off-axis loading (i.e., loading that does not happen along one of the principal axes of orthotropy of the material) are considered. Both previous examples highlighted the ability of the method to accurately predict size effects in notched composite laminates. However, these predictions referred to on-axis loading only. With respect to toughness, both present the same fracture toughness on the two principal axes of orthotropy and, for the QI one, no variation is seen. To the best of the authors' knowledge, there is no application where a model has been used at an ESL level to model the off-axis response and fracture of a MD, thin-ply laminate. The model presented is a first attempt in that direction by providing a means to account for fracture toughness variability in different orientations, and its accuracy is verified using the experimental results presented for off-axis OHT of a thin-ply laminate at 30°, 60° and 90° performed by Furtado et al. (2021).

The OHT specimens are in similar shape to that shown in Fig. 5(a) with $w = 36$ mm, $d = 12$ mm and have a nominal length of $L = 250$ mm. The material system of question is the T700/M21 75gsm thin-ply UD tape mentioned previously as H75 with the lay-up now being a hard laminate with the lay-up $[45/\text{-}45/0/45/\text{-}45/90/0/45/\text{-}45/90/0]_{\$}$ (the lay-up is center symmetric with the middle ply not repeating itself) giving the equivalent stiffnesses reported in Table 8. It is noted that, to achieve the results for loading in the off-axis direction, all that is required is an internal definition within Abaqus of the material orientation (i.e., assigning an orientation to the solid section of the material of the plate). Alternatively, this could be achieved by setting $\xi \neq 0$ (Eq. 16–17) and equal to the value of the off-axis angle of loading. Both procedures would render the same results.

By applying Eq. (20), the scaling constants come out to be $a_1 = -0.9171$ and $a_2 = -0.9399$. This produces the distribution of the fracture toughness seen in Fig. 11.

The numerical results for strength obtained are presented against the experimental values in Table 9. As can be observed, the predictions lie well within acceptable errors (under 5 %) with respect to the experimental data. It is noted that, once again, the strength of the on-axis test was used to obtain the optimal value of the length scale which for this laminate was $l = 0.8$ mm.

Looking at Fig. 11, that once again compares the fracture toughness as obtained via VCCT (please refer to Appendix A) and that assumed by

Table 5
Material properties for the T700/M21 lamina and cross-ply laminate.

	E_x(GPa)	E_y(GPa)	G_{xy}(GPa)	ν_{xy}
Lamina	146.6	8.7	4.6	0.34
Laminate	77.82	77.82	4.6	0.04

Table 6
Tested DENT specimen sizes.

	w(mm)	a_0(mm)	L(mm)
Size A	10	3	250
Size B	20	6	250
Size D	40	12	250
Size E	50	15	250

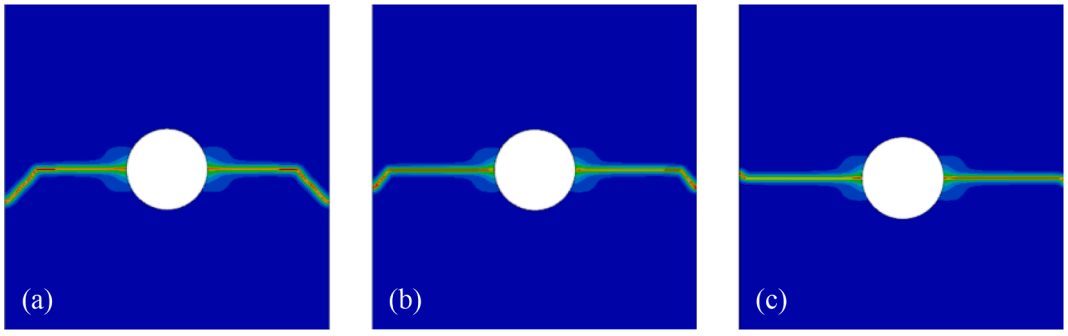

Fig. 8. Numerical fracture profiles for models with different lengths keeping all other analysis and geometrical parameters (width and hole diameter) constant: (a) original length, (b) length reduced to 50%, and (c) length reduced to 30%.

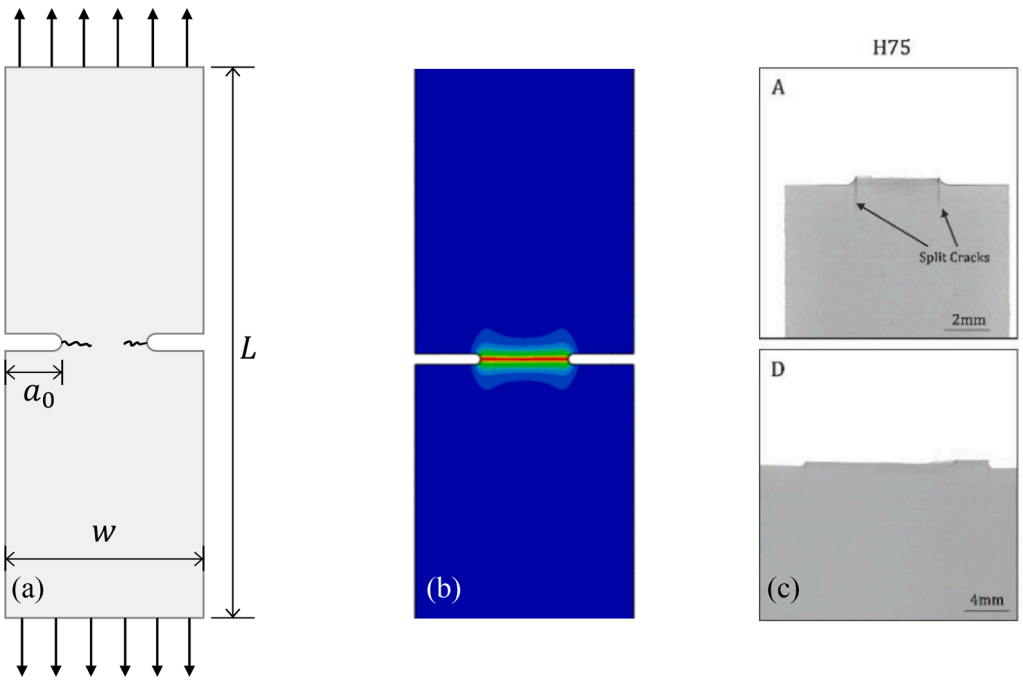

Fig. 9. (a) Schematic of the DENT specimen (b) typical numerical result (c) experimental crack pattern (Furtado et al., 2020).

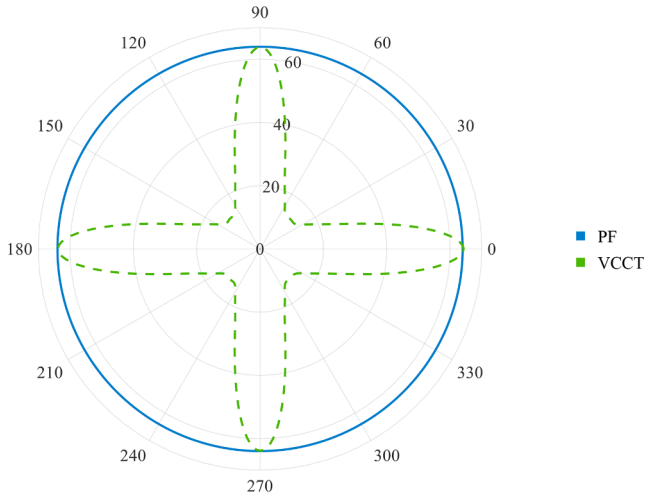

Fig. 10. Polar plot of the fracture toughness $G_c(\theta)$ that is assumed by the PF method and VCCT for the cross-ply laminate.

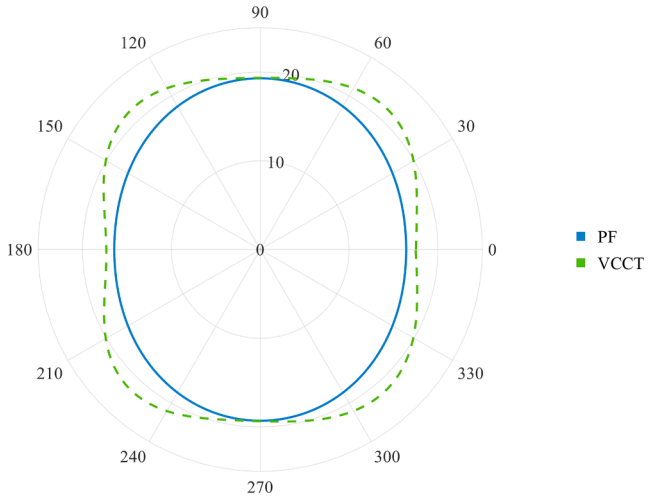

Fig. 11. Polar plot of the fracture toughness $G_c(\theta)$ that is assumed by the PF method and VCCT for the H75/hard laminate.

Table 7
DENT experimental and numerical results comparison.

	Experimental Av. (MPa)	FEA Prediction (MPa)	Error (%)
Size A	289.51	274.70	5.12
Size B	208.85	217.76	−4.27
Size D	164.56	164.54	0.01
Size E	136.11	147.19	−8.14

Table 8
Material properties for the t700/μ21 lamina and hard laminate.

	E_x(GPa)	E_y(GPa)	G_{xy}(GPa)	ν_{xy}
Lamina	146.6	8.7	4.6	0.34
Laminate	54.0	48.3	4.6	0.39

Table 9
Off-axis OHT experimental and numerical results comparison.

Off-axis angle	Experimental Av. (MPa)	FEA Prediction (MPa)	Error (%)
On-axis (0°)	333.00	319.98	4.07
30°	334.00	318.62	4.83
60°	301.00	315.20	−4.51
90°	302.00	305.87	−1.27

the PF formulation, this is not directly obvious as the fracture toughness distributions differ. But this difference is not of significant magnitude, contrary to the cross-ply case (Fig. 10) that has higher levels of anisotropy (with respect to fracture energy). In that case, the proposed model, based on second-order structural tensors to represent anisotropic fracture energy, is expected to "fail" for the off-axis cases. Thus, it is recognized that there must exist a limit of applicability of the model to

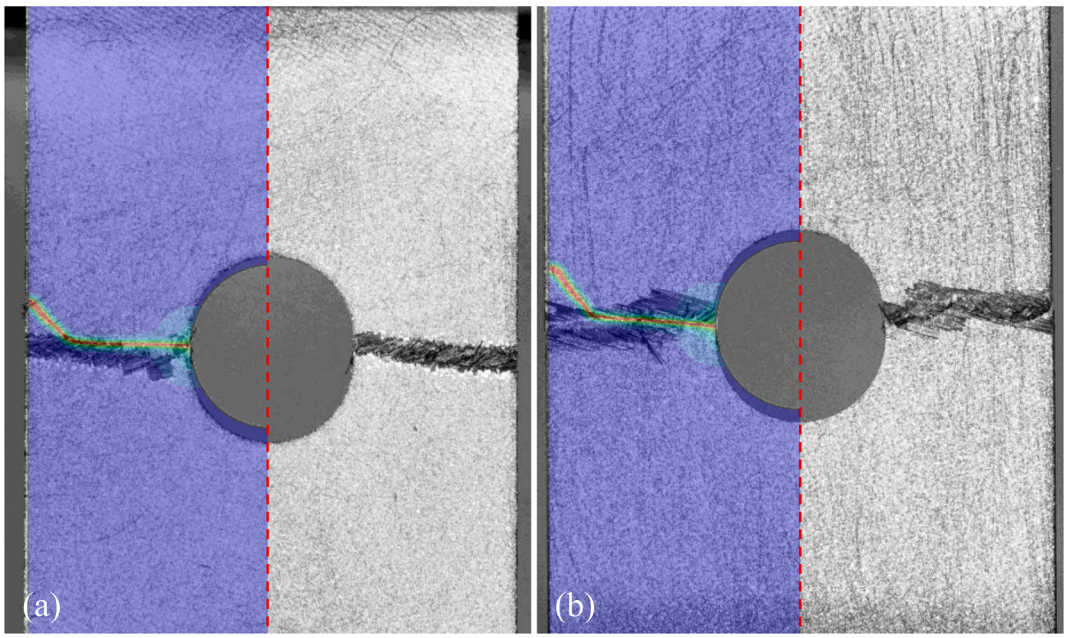

Fig. 12. Comparison of experimental and numerical crack paths for (a) 30o off-axis loading and (b) 60o off-axis loading.

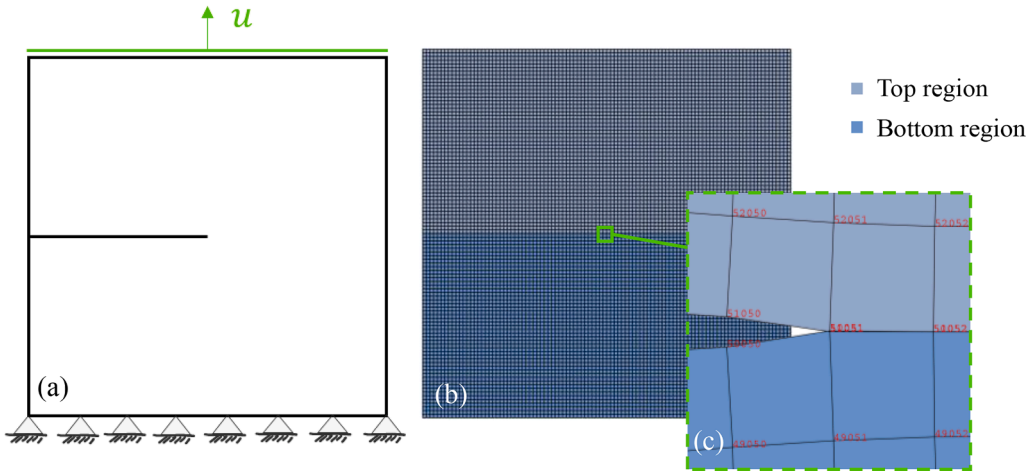

Fig. A1. Schematic of the (a) CT configuration (b) finite element model (c) close-up at the elements and nodes of the initial crack tip.

general loading cases for MD thin-ply laminates that present high levels of anisotropy with respect to fracture energy.

Finally, in the off-axis OHT testing it is noted that a crack profile that deviated from the horizontal axis (direction perpendicular to load application direction) was observed, contrary to isotropic or on-axis OHT results. As mentioned, the proposed PF model would not impose a fracture plane but rather obtain the crack angle as an output, and so, a comparison of the predicted fracture path to that obtained in the experiments for the 30° and 60° off-axis loading tests is presented in Fig. 12. The images are superposed on half of the face of the specimen (since the numerical result is symmetric along the center axis of the hole). This figure shows the satisfactory agreement of the crack path obtained by the proposed PF formulation (considering the initial trend of the crack while neglecting the near boundary regions) and that observed from the experiments. This highlights the necessity to include considerations of anisotropic fracture energy as an isotropic consideration would not be able to predict the slanted crack observed.

4. Conclusion and remarks

A new methodology to apply the PF method in an ESL approach to the case of fracture of balanced MD thin-ply laminates was developed. The proposed method entails redefining existing anisotropic PF formulations to obtain the parameters of the model using as inputs lamina properties and lay-up information, while also accounting for the variation of the fracture toughness in different laminate directions.

The second-order structural tensor of the anisotropic PF model, defined by scaled vectors of preferred material directions, was linked to the material symmetry and laminate fracture toughness, by defining a new formulation to obtain the scaling constants: using an analytical approach to calculate the fracture toughness of a MD laminate, the fracture toughness in two principal material directions is obtained, enabling the calculation of the scaling constants accordingly. The scaling constants, thus, become material dependent, something that consequently reduces the number of numerical parameters the model is dependent on. The methodology also significantly simplifies any calculations as well as test matrices required to obtain the inputs of the model as it only requires the lay-up and ply elastic properties and

fracture toughness and the definition of the length scale which is recognized to add an additional parameter.

The procedure is implemented for FEA using Abaqus, and a UMAT + UMATHT approach is followed. The UMATHT is used to include the anisotropic PF model via a UMAT approach while allowing the user to internally update and define the structural tensor. The code is available upon request.

To validate the proposed formulation, experimental results available in the literature were compared with those obtained from FEA. Two cases, OHT and DENT tests, demonstrated the ability of the proposed formulation to accurately capture size effects for MD laminates. Moreover, experimental data from off-axis OHT of a non-QI laminate were as well accurately captured. Both strength and crack path predictions lied well along the experimental results.

Future work includes the extension of this methodology, e.g., using higher order methods, to accurately capture the anisotropic fracture energy required to model in full the off-axis behavior of generally layered MD laminates of any level of anisotropy.

Declaration of Competing Interest

The authors declare that they have no known competing financial interests or personal relationships that could have appeared to influence the work reported in this paper.

Data availability

Data will be made available upon request.

Acknowledgements

The authors kindly acknowledge the funding received from the European Union's Horizon 2020 research and innovation programme under the Marie Skłodowska-Curie grant agreement No. 861061 – Project NEWFRAC under which this research is being executed. The second and fourth authors are also grateful for the support of FCT — Fundação para a Ciência e a Tecnologia, I.P., in the scope of the project UIDB/50022/2020. JR ackowledges the support of the Junta de Andalucía Consejería de Economía y Conocimiento, Junta de Andalucía, and European Regional Development Fund (Project P20-00595) and Ministerio de Ciencia e Innovación of Spain (Project TED2021-131649B-I00).

Appendix A:. Use of the VCCT to determine the fracture toughness of the laminate

The methodology proposed here, which assumes the orthotropic structural tensor for the crack density function, produces and can only assume an elliptical form for the distribution of the inverse of the fracture toughness. However, whether this is or is not representative of the actual realistic fracture toughness distribution is to be determined. In this work, the VCCT (Krueger, 2004) is used to obtain the fracture toughness of the laminates for various crack orientations with respect to the principal material axes. A compact tension (CT) configuration of unit length (1 mm edge) shown in Fig. A.1(a) was used and was simulated in Abaqus using the discretization shown in Fig. A.1(b). Each part of the CT specimen is separate, and they are bonded at the mid plane for half of the length for which in Abaqus a tie constraint of the surfaces is considered.

The material was assigned an orientation with respect to the crack orientation for which the fracture toughness is to be known. This was done for angles from 0° to 90° with increments of 5°. After the analysis was run for a certain value of the displacement, the respective ERR value is saved. Using as reference the ERR of the laminate at 0°, a ratio is calculated to produce the values of the fracture toughness for various angles. This was then fitted in MATLAB, using a sum of sines function with 8 terms (sin8), to produce the fracture toughness distribution form obtained by VCCT.

References

Abaqus 2020, 2019. Abaqus Theory Guide, Par. 2.11. Abaqus Documentation.
Ambati, M., Gerasimov, T., De Lorenzis, L., 2015. Phase-field modeling of ductile fracture. Comput. Mech. 55, 1017–1040. https://doi.org/10.1007/s00466-015-1151-4.
Arteiro, A., Catalanotti, G., Xavier, J., Camanho, P.P., 2013. Notched response of non-crimp fabric thin-ply laminates. Compos. Sci. Technol. 79, 97–114. https://doi.org/10.1016/J.COMPSCITECH.2013.02.001.
Arteiro, A., Catalanotti, G., Reinoso, J., Linde, P., Camanho, P.P., 2019. Simulation of the Mechanical Response of Thin-Ply Composites: From Computational Micro-Mechanics to Structural Analysis. Arch. Comput. Meth. Eng. 26, 1445–1487. https://doi.org/10.1007/s11831-018-9291-2.
Arteiro, A., Furtado, C., Catalanotti, G., Linde, P., Camanho, P.P., 2020. Thin-ply polymer composite materials: A review. Compos. A Appl. Sci. Manuf. 132, 105777 https://doi.org/10.1016/J.COMPOSITESA.2020.105777.
Bao, G., Ho, S., Suo, Z., Fan, B., 1992. The role of material orthotropy in fracture specimens for composites. Int. J. Solids Struct. 29, 1105–1116. https://doi.org/10.1016/0020-7683(92)90138-J.
Belytschko, T., Black, T., 1999. Elastic crack growth in finite elements with minimal remeshing. Int. J. Numer. Meth. Eng. 45, 601–620. https://doi.org/10.1002/(SICI)1097-0207(19990620)45:5<601::AID-NME598>3.0.CO;2-S.
Bleyer, J., Alessi, R., 2018. Phase-field modeling of anisotropic brittle fracture including several damage mechanisms. Comput. Methods Appl. Mech. Eng. 336, 213–236. https://doi.org/10.1016/J.CMA.2018.03.012.
Bourdin, B., Francfort, G.A., Marigo, J.J., 2000. Numerical experiments in revisited brittle fracture. J. Mech. Phys. Solids 48, 797–826. https://doi.org/10.1016/S0022-5096(99)00028-9.
Braun, M., Bischoff, M., Ramm, E., 1994. Nonlinear shell formulations for complete three-dimensional constitutive laws including composites and laminates. Comput. Mech. 15, 1–18. https://doi.org/10.1007/BF00350285.
Camanho, P.P., Catalanotti, G., 2011. On the relation between the mode I fracture toughness of a composite laminate and that of a 0° ply: Analytical model and experimental validation. Eng. Fract. Mech. 78, 2535–2546. https://doi.org/10.1016/J.ENGFRACMECH.2011.06.013.
Camanho, P.P., Erçin, G.H., Catalanotti, G., Mahdi, S., Linde, P., 2012. A finite fracture mechanics model for the prediction of the open-hole strength of composite laminates. Compos. A Appl. Sci. Manuf. 43, 1219–1225. https://doi.org/10.1016/J.COMPOSITESA.2012.03.004.
Carollo, V., Guillén-Hernández, T., Reinoso, J., Paggi, M., 2018. Recent advancements on the phase field approach to brittle fracture for heterogeneous materials and structures. Adv. Model Simul. Eng. Sci. 5, 8. https://doi.org/10.1186/s40323-018-0102-y.
Christensen, R.M., Zywicz, E., 1990. A Three-Dimensional Constitutive Theory for Fiber Composite Laminated Media. J. Appl. Mech. 57, 948–955. https://doi.org/10.1115/1.2897666.
Clayton, J.D., Knap, J., 2015. Phase field modeling of directional fracture in anisotropic polycrystals. Comput. Mater. Sci 98, 158–169. https://doi.org/10.1016/J.COMMATSCI.2014.11.009.
Francfort, G.A., Marigo, J.J., 1998. Revisiting brittle fracture as an energy minimization problem. J. Mech. Phys. Solids 46, 1319–1342. https://doi.org/10.1016/S0022-5096(98)00034-9.
Furtado, C., Arteiro, A., Linde, P., Wardle, B.L., Camanho, P.P., 2020. Is there a ply thickness effect on the mode I intralaminar fracture toughness of composite laminates? Theor. Appl. Fract. Mech. 107, 102473 https://doi.org/10.1016/J.TAFMEC.2020.102473.
Furtado, C., Tavares, R.P., Arteiro, A., Xavier, J., Linde, P., Wardle, B.L., Camanho, P.P., 2021. Effects of ply thickness and architecture on the strength of composite sub-structures. Compos. Struct. 256, 113061 https://doi.org/10.1016/J.COMPSTRUCT.2020.113061.
Iarve, E.V., Gurvich, M.R., Mollenhauer, D.H., Rose, C.A., Dávila, C.G., 2011. Mesh-independent matrix cracking and delamination modeling in laminated composites. Int. J. Numer. Meth. Eng. 88, 749–773. https://doi.org/10.1002/nme.3195.
Kawabe, K., Matsuo, T., Maekawa, Z.-I., 1998. New Technology for Opening Various Reinforcing Fiber Tows. J. Soc. Mater. Sci., Jpn. 47 (7), 727–734.
Krueger, R., 2004. Virtual crack closure technique: History, approach, and applications. Appl. Mech. Rev. 57, 109–143. https://doi.org/10.1115/1.1595677.
Laux, T., Gan, K.W., Tavares, R.P., Furtado, C., Arteiro, A., Camanho, P.P., Thomsen, O. T., Dulieu-Barton, J.M., 2021. Modelling damage in multidirectional laminates subjected to multi-axial loading: Ply thickness effects and model assessment. Compos. Struct. 266, 113766 https://doi.org/10.1016/J.COMPSTRUCT.2021.113766.
Li, B., Maurini, C., 2019. Crack kinking in a variational phase-field model of brittle fracture with strongly anisotropic surface energy. J. Mech. Phys. Solids 125, 502–522. https://doi.org/10.1016/j.jmps.2019.01.010.
Li, B., Peco, C., Millán, D., Arias, I., Arroyo, M., 2015. Phase-field modeling and simulation of fracture in brittle materials with strongly anisotropic surface energy. Int. J. Numer. Meth. Eng. 102, 711–727. https://doi.org/10.1002/nme.4726.
Lorentz, E., 2017. A nonlocal damage model for plain concrete consistent with cohesive fracture. Int. J. Fract. 207, 123–159. https://doi.org/10.1007/s10704-017-0225-z.
Maimí, P., Camanho, P.P., Mayugo, J.A., Dávila, C.G., 2007. A continuum damage model for composite laminates: Part I - Constitutive model. Mech. Mater. 39, 897–908. https://doi.org/10.1016/J.MECHMAT.2007.03.005.
Moes, N., Dolbow, J., Belytschko, T., 1999. A finite element method for crack growth without remeshing. Int. J. Numer. Meth. Eng. 46, 131–150. https://doi.org/10.1002/(SICI)1097-0207(19990910)46:1<131::AID-NME726>3.0.CO;2-J.

Molnár, G., Doitrand, A., Estevez, R., Gravouil, A., 2020. Toughness or strength? Regularization in phase-field fracture explained by the coupled criterion. Theor. Appl. Fract. Mech. 109, 102736 https://doi.org/10.1016/j.tafmec.2020.102736.

Navidtehrani, Y., Betegón, C., Martínez-Pañeda, E., 2021. A simple and robust Abaqus implementation of the phase field fracture method. Applications in Engineering Science 6, 100050. https://doi.org/10.1016/J.APPLES.2021.100050.

Nguyen, T.-T., Réthoré, J., Yvonnet, J., Baietto, M.-C., 2017. Multi-phase-field modeling of anisotropic crack propagation for polycrystalline materials. Comput. Mech. 60, 289–314. https://doi.org/10.1007/s00466-017-1409-0.

Pham, K., Amor, H., Marigo, J.-J., Maurini, C., 2011. Gradient Damage Models and Their Use to Approximate Brittle Fracture. Int. J. Damage Mech 20, 618–652. https://doi.org/10.1177/1056789510386852.

Pillai, U., Triantafyllou, S.P., Essa, Y., de la Escalera, F.M., 2020. An anisotropic cohesive phase field model for quasi-brittle fractures in thin fibre-reinforced composites. Compos. Struct. 252, 112635.

Quintanas-Corominas, A., Reinoso, J., Casoni, E., Turon, A., Mayugo, J.A., 2019. A phase field approach to simulate intralaminar and translaminar fracture in long fiber composite materials. Compos. Struct. 220, 899–911. https://doi.org/10.1016/J.COMPSTRUCT.2019.02.007.

Raina, A., Miehe, C., 2016. A phase-field model for fracture in biological tissues. Biomech. Model. Mechanobiol. 15, 479–496. https://doi.org/10.1007/s10237-015-0702-0.

Reifsnider, K.L., Iarve, E.V., Raihan, R., Adluru, H.K., Hoos, K.H., 2020. Durability of aerospace material systems. Durability of Composite Systems 107–163. https://doi.org/10.1016/B978-0-12-818260-4.00003-X.

Reinoso, J., Arteiro, A., Paggi, M., Camanho, P.P., 2017. Strength prediction of notched thin ply laminates using finite fracture mechanics and the phase field approach. Compos. Sci. Technol. 150, 205–216. https://doi.org/10.1016/J.COMPSCITECH.2017.07.020.

Scherer, J.-M., Brach, S., Bleyer, J., 2022. An assessment of anisotropic phase-field models of brittle fracture. Comput. Methods Appl. Mech. Eng. 395, 115036 https://doi.org/10.1016/j.cma.2022.115036.

Schuecker, C., Pettermann, H.E., 2006. A continuum damage model for fiber reinforced laminates based on ply failure mechanisms. Compos. Struct. 76, 162–173. https://doi.org/10.1016/J.COMPSTRUCT.2006.06.023.

Sihn, S., Kim, R.Y., Kawabe, K., Tsai, S.W., 2007. Experimental studies of thin-ply laminated composites. Compos. Sci. Technol. 67, 996–1008. https://doi.org/10.1016/J.COMPSCITECH.2006.06.008.

Sun, C.T., Li, S., 1988. Three-Dimensional Effective Elastic Constants for Thick Laminates. J. Compos. Mater. 22, 629–639. https://doi.org/10.1177/002199838802200703.

Tanné, E., Li, T., Bourdin, B., Marigo, J.J., Maurini, C., 2018. Crack nucleation in variational phase-field models of brittle fracture. J. Mech. Phys. Solids 110, 80–99. https://doi.org/10.1016/J.JMPS.2017.09.006.

Teichtmeister, S., Kienle, D., Aldakheel, F., Keip, M.A., 2017. Phase field modeling of fracture in anisotropic brittle solids. Int. J. Non Linear Mech. 97, 1–21. https://doi.org/10.1016/J.IJNONLINMEC.2017.06.018.

Tsai, S.W., 2021. Double–Double: New Family of Composite Laminates. AIAA J. 59, 4293–4305. https://doi.org/10.2514/1.J060659.

Tsai, S., Sihn, S., Kim, R., 2005. Thin Ply Composites. In: 46th AIAA/ASME/ASCE/AHS/ASC Structures, Structural Dynamics and Materials Conference. American Institute of Aeronautics and Astronautics, Reston, Virigina. https://doi.org/10.2514/6.2005-2005.

Turon, A., Camanho, P.P., Costa, J., Dávila, C.G., 2006. A damage model for the simulation of delamination in advanced composites under variable-mode loading. Mech. Mater. 38, 1072–1089. https://doi.org/10.1016/J.MECHMAT.2005.10.003.

van der Meer, F.P., Oliver, C., Sluys, L.J., 2010. Computational analysis of progressive failure in a notched laminate including shear nonlinearity and fiber failure. Compos. Sci. Technol. 70, 692–700. https://doi.org/10.1016/J.COMPSCITECH.2010.01.003.

Whitney, J.M., Nuismer, R.J., 1974. Stress Fracture Criteria for Laminated Composites Containing Stress Concentrations. J. Compos. Mater. 8, 253–265. https://doi.org/10.1177/002199837400800303.

Wu, J.-Y., 2017. A unified phase-field theory for the mechanics of damage and quasi-brittle failure. J. Mech. Phys. Solids 103, 72–99. https://doi.org/10.1016/j.jmps.2017.03.015.

Yokozeki, T., Kuroda, A., Yoshimura, A., Ogasawara, T., Aoki, T., 2010. Damage characterization in thin-ply composite laminates under out-of-plane transverse loadings. Compos. Struct. 93, 49–57. https://doi.org/10.1016/J.COMPSTRUCT.2010.06.016.